

Enhancing the Performance of Textile Triboelectric Nanogenerators with Oblique Microrod Arrays for Wearable Energy Harvesting

Lu Zhang,^{†,‡} Chen Su,[†] Li Cheng,[†] Nuanyang Cui,^{†,‡} Long Gu,^{†,‡} Yong Qin,^{*,†} Rusen Yang,^{*,‡} and Feng Zhou[§]

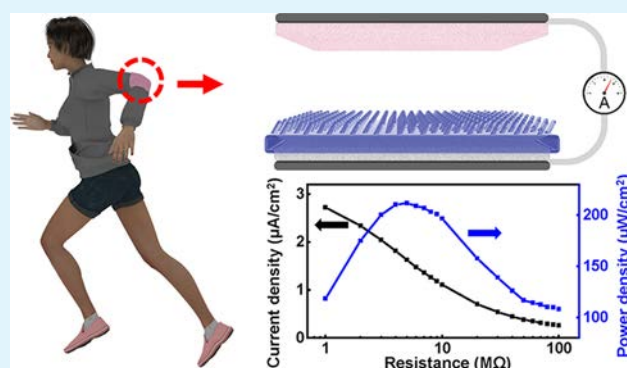
[†]Institute of Nanoscience and Nanotechnology, Lanzhou University, Lanzhou 730000, China

[‡]School of Advanced Materials and Nanotechnology, Xidian University, Xi'an 710071, China

[§]State Key Laboratory of Solid Lubrication, Lanzhou Institute of Chemical Physics, Chinese Academy of Sciences, Lanzhou 730000, China

ABSTRACT: The rapid development of wearable electronics urgently requires a wearable energy-harvesting technology that can convert mechanical energy from body movements into electricity. In this paper, a novel structure with an oblique microrod array is employed to fabricate a high-performance textile-based wearable triboelectric nanogenerator (WTNG). The contact area of WTNGs can be efficiently enhanced when the oblique poly(dimethylsiloxane) microrods are forced to bend uniformly and slide along one direction during the working condition. The oblique microrod structure enables the WTNG to generate a short-circuit current density and an open-circuit voltage reaching $3.24 \mu\text{A}/\text{cm}^2$ and 1014.2 V , respectively. The maximum peak power density of a WTNG reached $211.7 \mu\text{W}/\text{cm}^2$. Meanwhile, 48 red light-emitting diodes were simultaneously lit up by tapping a WTNG. Furthermore, the WTNG can be dressed on an elbow to continuously harvest energy from human motions as a sustainable power source. This work develops an efficient approach for enhancing the output performance of triboelectric nanogenerators and paves a promising way to power wearable electronics.

KEYWORDS: oblique microrod array, triboelectric nanogenerator, mechanical energy, energy-harvesting, wearable electronic



1. INTRODUCTION

In recent years, a pervasive concept of “wearable electronics” has attracted tremendous research interest. Owing to the merits of miniaturization, portability, and multifunctionality, their application provides sufficient convenience for consumers’ daily life such as making a call, video chatting, surfing the internet, and health-monitoring.^{1–4} Unlike current electronics, the wearable electronics can integrate many functional devices with a powerful and flexible energy source. To date, the most wearable devices are sustained with conventional electrochemical batteries, which are extremely restricted by the lifetime, sustainable operation, and environment issues.^{5,6} In these cases, developing a new type of power source is in urgent demand for self-powered wearable electronics, which can continuously scavenge mechanical energy from ambient environment and be well-suited for wearable electronics.

Compared to the extensively studied mechanical energies including wind energy,^{7–9} sound wave energy,^{10,11} vibration energy,¹² and tide energy,^{13,14} mechanical energy from human motions is a reliable and sustainable power source that is available almost anywhere and anytime without environmental and geographical constraints. For example, approximately 100 W energy of an adult is consumed in fueling motions such as

walking, arm swinging, finger motion, heart beats, and so on.^{15,16} Only 1% of this energy is enough to power most portable and personal wearable electronics. For example, transmitting data in common M2M (Machine-to-Machine) scenarios via Bluetooth needs only 1–10 mW of power.¹⁷ Mobile phones typically need just over 1 W of power on average.¹⁸ Recently, a new type of triboelectric nanogenerator (TENG) has been widely reported to efficiently harvest energy from the surrounding environment due to its simplicity, cost-effectiveness, reliability and environmental friendliness.^{19,20} Its work mechanism lies in the couple of triboelectrification and electrostatic induction.²¹ Up till now, many designs have been demonstrated to convert the mechanical energy of human motion into electricity for portable electronics, such as the TENG with a “grating structure” to harvest arm-swing energy to power tubelike lamps,²² weaving craft for self-charging power textiles for wearable electronics,²³ eye-motion-triggered TENG for mechnosensational communication systems,²⁴ circular-type TENG for electronic hearing systems,²⁵ and

Received: April 16, 2019

Accepted: July 4, 2019

Published: July 4, 2019

intergrated charge excitation TENG for lighting white light-emitting diodes (LEDs),²⁶ all of which have proven the feasibility of TENG to harvest the mechanical energy of human motions. Although different micro-/nanostructures have been fabricated to enhance the output performance of the WTNGs such as nanoparticles, nanowires, and mesoporous materials,^{27–29} an optimized structure design is still lacking. Hence, it is important to design an optimized structure for a highly efficient WTNG for mechanical energy-harvesting.

In this work, we designed a simple approach to fabricate oblique microrod arrays to enhance the output performance of a WTNG, where the oblique poly(dimethylsiloxane) (PDMS) microrod array was fabricated in situ on the surface of a textile through inclined lithography and template transfer. Here, the work mechanism of the oblique microrod array is illustrated in detail and compared with a conventional structure. When the WTNG was driven by a regular mechanical force, a maximum short-circuit current density of $3.24 \mu\text{A}/\text{cm}^2$, a maximum open-circuit voltage of 1014.2 V, and a maximum instantaneous electric output power density of $211.7 \mu\text{W}/\text{cm}^2$ were reached. Furthermore, 48 red LEDs were simultaneously lit by the WTNG. A WTNG was sewed on a piece of fabric and an elbow supporter, which were triggered by tensile forces and elbow movements respectively to scavenge energy from human motions, and produced short-circuit currents of 12.5 and $3.6 \mu\text{A}$, respectively.

2. EXPERIMENTAL SECTION

2.1. Fabrication of Nanowire Arrays on the Surface of a Fabric. Nanowire arrays on the surface of a nylon fabric were fabricated by direct reactive ion-etching (RIE) without nanopatterns or prefabricated masks, which have been concretely demonstrated in our previous work.³⁰ In this work, the nylon fabric was first put on the bottom electrode of the RIE machine and then covered over by a Faraday cage consisting of a Cu grid top plane and a Cu sidewall. After the chamber of RIE was vacuumized to 4×10^{-4} Pa, the nylon fabric was etched under conditions of 60 sccm O_2 gas flow, 2 Pa pressure, and 100 W input power. After 5 min of etching, the nanowire array was evenly distributed on the surface of the nylon fabric and the length of the nanowire array was controlled by adjusting the etching time.

2.2. Fabrication of Oblique PDMS Microrod Arrays. The fabrication process of oblique PDMS microrod arrays includes inclined lithography and template transfer. First, a negative photoresist layer was spin-coated on a glass sheet ($4 \text{ cm} \times 4 \text{ cm}$) with about $30 \mu\text{m}$ thickness at a speed of 1500 rpm for 30 s. Then, the photoresist-coated glass sheet was baked on a hotplate for 3 min at 150°C . Subsequently, the glass sheet was located at an angle of 30° with respect to the flat surface and exposed to UV light ($2.2 \text{ mW}/\text{cm}^2$) for 50 s. After inclined lithography, the photoresist was soaked in a developer for 3–5 min and then baked on a hotplate for 5 min at 90°C ; the array of oblique openings was finally formed on the surface of the glass sheet.

The glass sheet with a patterned photoresist layer worked as a template in the fabrication process, and PDMS (Sylgard 184, Dow Corning) was used as the imprinted polymer. The base monomer and the cross-linker of PDMS were mixed in a 10:1 ratio (w/w) and then evenly cast on the template. A piece of spandex fabric was subsequently paved on the template with PDMS. The residual air existing in the PDMS was removed in a vacuum chamber. During the process, the PDMS solution gradually penetrated into the space between the fibers of the fabric and the oblique openings in the template, and so the two materials firmly attached to each other. After a thermal curing process at 80°C for 1 h, the PDMS film with oblique microrod arrays was peeled off from the template, and the template could be reused.

2.3. Characterization and Measurement. Field-emission SEM (Hitachi S4800) was employed to characterize the surface morphologies of the nano-/microstructures on the surface of fabrics. To test the electric output of the WTNG based on oblique microrod arrays, a linear motor (LinMot E1100) was used to produce periodic alternative motions and drive the two parts of the WTNG to contact and separate. Meanwhile, preamplifiers (SR570, SR560) were used to measure the open-circuit voltage and short-circuit current. Moreover, PCI-6259 (National Instruments) was used for data collection. A software platform based on LabVIEW was used to realize real-time data acquisition and analysis.

3. RESULTS AND DISCUSSION

To realize the energy-harvesting from human motions as shown in Figure 1a, the schematic structure of our WTNG is

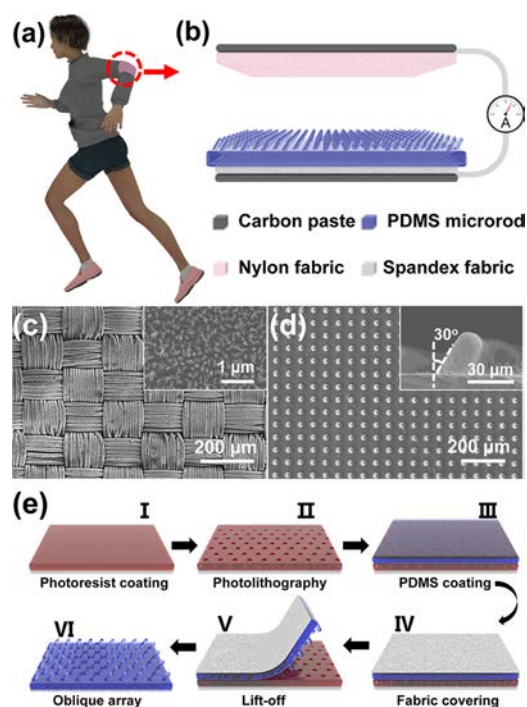


Figure 1. Structural design of a WTNG to harvest mechanical energy from human motions. (a) Schematic diagram of a WTNG sewed on the cloth near an elbow. (b) Structure of the WTNG. (c) SEM image of a nylon fabric with nanowires. Inset is a partial enlargement of nanowires. (d) Top-view SEM image of uniform oblique PDMS microrod arrays. The inset is the side-view SEM image of a PDMS microrod. The angle between the microrod and the normal is 30° . (e) Flowchart of the fabrication process of the oblique PDMS microrod array on a spandex fabric. Steps I and II describe the preparation of the template with oblique openings on the glass substrate by inclined photolithography. Steps III to VI describe the fabrication of the oblique PDMS microrod array on a spandex fabric duplicating from the template.

designed to work in the traditional contact-separation mode shown in Figure 1b. The WTNG consists of a piece of nylon fabric and a piece of spandex fabric. To enhance the performance of WTNG, oblique PDMS microrod arrays and polymer nanowires were fabricated on the surface of spandex and nylon fabrics, respectively. Both polymer nanowires on the nylon surface and PDMS microrod arrays on the spandex fabric were chosen as the friction surfaces. On the back of the two fabrics, a carbon paste was painted to serve as electrodes, which were connected with an external Cu wire. In Figure 1c,

the SEM image shows that the nylon fabric is woven with many fibers with a diameter of about 10 μm . The inset shows that the etched nanowires are evenly distributed on the fabric surface with a diameter of about 30–50 nm. The experimental details are provided in the [Experimental Section](#). [Figure 1d](#) shows a regular oblique PDMS microrod array distributed on the spandex fabric surface; the distance between two microrods is approximately 40 μm . The inset in [Figure 1d](#) shows the cross-sectional SEM image of a PDMS microrod depicting that the microrod is about 25 μm in diameter, 30 μm in length, and at 30° with the normal direction. The detailed fabrication process of oblique PDMS microrod arrays on the spandex fabric surface is schematically shown in [Figure 1e](#), which can be mainly divided into two processes. The first process is to fabricate a template with an oblique hollow cylindrical array from steps I to II, and the second process is the transfer of the oblique cylindrical array to the surface of the spandex fabrics from steps III to VI. The detailed description of the fabrication process is given in the [Experimental Section](#). During the transferring process, the PDMS solution can gradually penetrate into the space between the fibers of the fabric, ensuring that the flexible spandex fabric and the viscous PDMS can firmly combine together to form a unified whole, which can not only keep the flexibility of the fabric but also bear the fierce strain-driven modes.

To explore its electrical output performance, the WTNG was deformed at a frequency of 5 Hz and an amplitude of 10 mm. All of the measurements in this work were conducted under the same conditions with a relative humidity of 30% and a temperature of 16 °C. [Figure 2a,b](#) shows the maximum short-

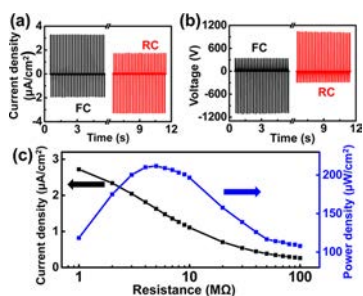


Figure 2. Electrical output performance of a WTNG driven by periodic external forces. (a) Short-circuit current with forward connection (FC) on the left half and reverse connection (RC) on the right half. (b) Open-circuit voltage with FC on the left half and RC on the right half. (c) Output current (left axis) and instantaneous electric power (right axis) as a function of the external load resistance.

circuit current density of 3.24 $\mu\text{A}/\text{cm}^2$ and the open-circuit voltage of 1014.2 V, respectively. During the measurement, the FC (forward connection) and RC (reverse connection) between the WTNG and the external circuit were employed to rule out system artifacts. As shown in [Figure 2a,b](#), the corresponding outputs of the FC and RC have opposite signs and approximately same values, verifying that the output was indeed from the WTNG. [Figure 2c](#) shows the external resistance dependence of both the output current and the instantaneous electrical output power density, where the power density was calculated based on the equation $P = I^2R/S$ (I , R , and S stand for the current, load resistance, and friction area, respectively). With the increase of load resistance, the peak current value decreases mainly due to the ohmic loss. On the contrary, the instantaneous peak power density increases at

first and then decreases, where the maximum instantaneous power density can reach 211.7 $\mu\text{W}/\text{cm}^2$ at a load resistance of 6 M Ω .

To check the influence of the oblique PDMS microrod array on the nanogenerator performance, three additional devices with different top layers were prepared to act as the control groups. In these control groups, the oblique PDMS microrod array was replaced by a naked spandex fabric without any treatment ([Figure 3a](#)), a flat PDMS film ([Figure 3b](#)), and

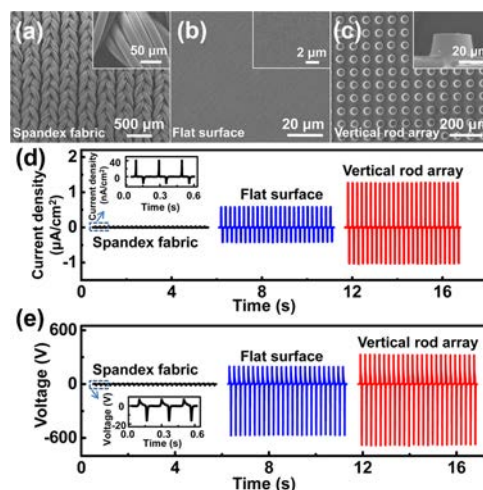


Figure 3. Comparative tests of nanogenerators with different top layers. (a–c) SEM images of the materials in place of the oblique PDMS microrod array in the control group including the naked spandex fabric (a), flat PDMS film on the spandex fabric (b) and vertical PDMS microrod array on the spandex fabric (c). (d) Short-circuit current of nanogenerators in the control group measured under the same conditions. Inset: enlarged view of three cycles. (e) Open-circuit voltage of nanogenerators in the control group measured under the same conditions. Inset: enlarged view of three cycles.

vertical PDMS microrod arrays ([Figure 3c](#)). [Figure 3d,e](#) shows the electrical output performance of these control groups including the short-circuit current and the open-circuit voltage. The output performance of four kinds of WTNGs are summarized in [Table 1](#). The corresponding inductive charges

Table 1. Statistics of the Short-Circuit Current, Open-Circuit Voltage, and Inductive Charge per Peak of the WTNG Under the Same Working Conditions

| | short-circuit current ($\mu\text{A}/\text{cm}^2$) | open-circuit voltage (V) | inductive charge density (nC/cm^2) |
|---------------------|-----------------------------------------------------|--------------------------|------------------------------------------------------|
| spandex fabric | 0.02 | 16.1 | 0.09 |
| flat surface | 0.57 | 569.6 | 3.19 |
| vertical rod arrays | 1.26 | 684.2 | 5.58 |
| oblique rod arrays | 3.24 | 1014.2 | 10.28 |

are calculated by integrating one cycle of the short-circuit current. The results in [Table 1](#) show that the outputs largely increased as the top layer changes from the naked spandex fabric, flat PDMS film, and vertical PDMS microrod array to the oblique PDMS microrod array. The short-circuit current density increased from 0.02 to 3.24 $\mu\text{A}/\text{cm}^2$, the open-circuit voltage increased from 16.1 to 1014.2 V, and the inductive charge density increased from 0.09 to 10.28 nC/cm^2 .

Comparing the outputs of nanogenerators using the naked spandex fabric with those using the flat PDMS film, PDMS is found to obtain more electrons than the spandex fabric. A comparison of the outputs of nanogenerators with the flat PDMS film and those with the vertical PDMS microrod array reveals that the oblique microrod array plays an important role in enhancing the output of WTNG due to an enhanced friction area. Furthermore, a comparison of the outputs of nanogenerators with a vertical PDMS microrod array and those with an oblique PDMS microrod array shows that the oblique microrod array structure has a much more enhanced output performance than the vertical PDMS microrod array.

The operating mechanism of the WTNG is explained by the coupling of the triboelectric effect and electrostatic effect, which has been concretely depicted in previous works.^{31,32} The reason why there is a big difference in output performances of the vertical PDMS microrod array and the oblique PDMS microrod array is explained in Figure 4. As shown in Figure 4a,

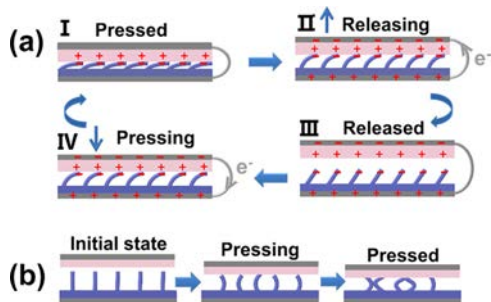


Figure 4. Working mechanisms of WTNGs based on (a) oblique microrod arrays and (b) vertical microrod arrays.

the oblique microrod array is much easier to be bent along one direction when two friction layers are forced to come in contact with each other and the microrods further slide along the nylon surface. In this work mode, the effective contact area is enhanced due to the additional slide friction of microrods and much more triboelectric charge is produced on the friction surface. However, in comparison, the vertical microrods bend randomly, where some rods can even collide with each other, limiting their further movement (Figure 4b), and further affect the enhancement of the output performance. The important role of the oblique PDMS microrod array in enhancing the WTNG output performance indicates that better designed microstructures can markedly improve the output performance of TENGs.

Furthermore, we also performed the durability test of a WTNG for practical application. During the test, the WTNG was continuously driven for 3 h (over 12 000 cycles) by a linear motor. Figure 5a shows that there is no obvious change in the output current density throughout the test. The partially enlarged views of the first 20 s (Figure 5b) and the last 20 s (Figure 5c) show that the output current density remains at about $3.0 \mu\text{A}/\text{cm}^2$ and the WTNG shows good stability under long-term testing. In our daily life, there are many sources of mechanical energy from every part of the human body such as knee-joints, shoulders, and elbows, which result in the stretching and releasing processes of clothes. It is valuable to check if our WTNG can effectively harvest these body movements. As shown in Figure 5d, the WTNG and 48 red LEDs were connected in series. At first, the red LEDs are dark

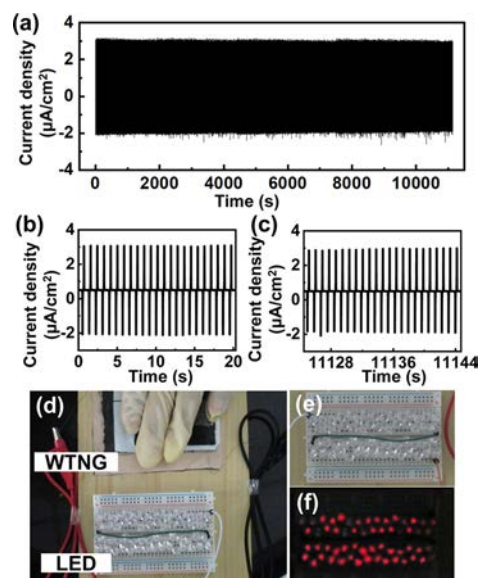


Figure 5. Durability test of a WTNG and its application for driving 48 LEDs. (a) High-stability test of WTNG under 3 h of operation (over 12 000 cycles). (b, c) Partially enlarged views of the first 20 s and the last 20 s, respectively. (d) Photograph of the WTNG driving 48 LEDs by tapping. (e, f) LEDs without and with the electricity generated by the WTNG, respectively.

in Figure 5e. With continuous tapping on the WTNG, all of the LEDs were lit up simultaneously (Figure 5f).

At last, the WTNG was sewed on clothes to check its ability to convert the mechanical energy of the motions of human clothes into electric energy and two driven modes were demonstrated in this work. When the fabric was stretched and released by hand (Figure 6a,b), the two parts of the WTNG experienced the contact-separation process and the WTNG

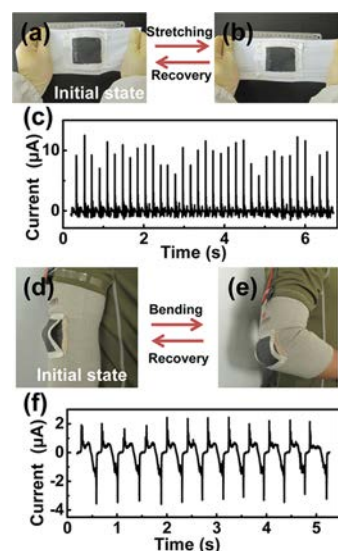


Figure 6. WTNG sewed on a piece of spandex fabric driven by hands and the WTNG sewed on an elbow supporter driven by a human elbow. (a, b) Optical images of the stretching and releasing states, respectively. (c) Short-circuit current of a WTNG under this driven mode. Inset: enlarged view of one peak. (d, e) Optical images of the bending and releasing states, respectively. (f) Short-circuit current of the WTNG under this driven mode. The elbow was bending at an angle of about 90° .

generated electric energy. Figure 6c shows that the short-circuit current of the WTNG reaches $12.5 \mu\text{A}$ under this strain-driven mode. Finally, the WTNG was sewed onto an elbow supporter to test its performance driven by human elbow movements. As shown in Figure 6d,e, the elbow supporter with a WTNG is dressed on a human arm and the WTNG faces toward the elbow completely. When the elbow is bent to an angle of about 90° , the two parts of the WTNG are forced to come in close contact with each other. In accordance with the elbow's action, the short-circuit current of the WTNG reaches $3.6 \mu\text{A}$ under this driven mode (Figure 6f). This result indicates that the WTNG can work under different driven modes. The output power is lower than that of a WTNG driven by a linear motor because of the smaller active area and lower driving speed. Our experiments have proven that it is feasible and practical to fabricate a WTNG harvesting energy from human motions, which gives a new approach to enhance the WTNG performance by optimizing its structure.

4. CONCLUSIONS

In summary, we have designed and fabricated novel oblique PDMS microrod arrays on a textile to enhance the performance of a WTNG for harvesting mechanical energy from human motions. When driven by a linear motor, the short-circuit current density and the open-circuit voltage of the WTNG reached $3.24 \mu\text{A}/\text{cm}^2$ and 1014.2 V , respectively. The maximum instantaneous electric output power density was up to $211.7 \mu\text{W}/\text{cm}^2$. Meanwhile, the WTNG shows good stability under long-term testing. Finally, the WTNG was sewed on clothes, and the short-circuit current reached 12.5 and $3.6 \mu\text{A}$ under the two different driven modes of tapping and stretching, respectively. The novel oblique polymer nanowire array provides an effective way for WTNGs to harvest energy from activities to act as a stable and sustainable power source.

AUTHOR INFORMATION

Corresponding Authors

*E-mail: qinyong@lzu.edu.cn (Y.Q.).

*E-mail: rsyang@xidian.edu.cn (R.Y.).

ORCID

Yong Qin: 0000-0002-6713-480X

Rusen Yang: 0000-0002-4019-4642

Feng Zhou: 0000-0001-7136-9233

Author Contributions

This manuscript was written through contributions of all authors. All authors have given approval to the final version of the manuscript.

Notes

The authors declare no competing financial interest.

ACKNOWLEDGMENTS

We sincerely appreciate the support from NSFC (Nos. 51472111, 81801847, 51603162, and 51702377), the Fundamental Research Funds for the Central Universities (No. JB181403, lzujbky-2018-ot04), the National Program for Support of Top-notch Young Professionals, and the National Natural Science Foundation of Shaanxi Province under Grant No. 2019JQ-291, 2019JQ-007.

REFERENCES

- (1) Wang, Z. L.; Wu, W. Nanotechnology-Enabled Energy Harvesting for Self-Powered Micro-/Nanosystems. *Angew. Chem., Int. Ed.* **2012**, *51*, 11700–11721.
- (2) Wang, Z. L. Self-Powered Nanosensors and Nanosystems. *Adv. Mater.* **2012**, *24*, 280–285.
- (3) Kou, L.; Huang, T.; Zheng, B.; Han, Y.; Zhao, X.; Gopalsamy, K.; Sun, H.; Gao, C. Coaxial Wet-Spun Yarn Supercapacitors for High-Energy Density and Safe Wearable Electronics. *Nat. Commun.* **2014**, *5*, No. 3754.
- (4) Son, D.; Lee, J.; Qiao, S.; Ghaffari, R.; Kim, J.; Lee, J. E.; Song, C.; Kim, S. J.; Lee, D. J.; Jun, S. W.; Yang, S.; Park, M.; Shin, J.; Do, K.; Lee, M.; Kang, K.; Hwang, C. S.; Lu, N.; Hyeon, T.; Kim, D.-H. Multifunctional Wearable Devices for Diagnosis and Therapy of Movement Disorders. *Nat. Nanotechnol.* **2014**, *9*, 397–404.
- (5) Xu, C.; Zi, Y.; Wang, A. C.; Zou, H.; Dai, Y.; He, X.; Wang, P.; Wang, Y.-C.; Feng, P.; Li, D.; Wang, Z. L. On the Electron-Transfer Mechanism in the Contact-Electrification Effect. *Adv. Mater.* **2018**, *30*, No. 1706790.
- (6) Chen, B.; Tang, W.; Jiang, T.; Zhu, L.; Chen, X.; He, C.; Xu, L.; Guo, H.; Lin, P.; Li, D.; Shao, J.; Wang, Z. L. Three-Dimensional Ultraflexible Triboelectric Nanogenerator Made by 3D Printing. *Nano Energy* **2018**, *45*, 380–389.
- (7) Lee, S.; Bae, S.-H.; Lin, L.; Yang, Y.; Park, C.; Kim, S.-W.; Cha, S. N.; Kim, H.; Park, Y. J.; Wang, Z. L. Super-Flexible Nanogenerator for Energy Harvesting from Gentle Wind and as an Active Deformation Sensor. *Adv. Funct. Mater.* **2013**, *23*, 2445–2449.
- (8) Bai, S.; Zhang, L.; Xu, Q.; Zheng, Y.; Qin, Y.; Wang, Z. L. Two Dimensional Woven Nanogenerator. *Nano Energy* **2013**, *2*, 749–753.
- (9) Xie, Y.; Wang, S.; Lin, L.; Jing, Q.; Lin, Z.-H.; Niu, S.; Wu, Z.; Wang, Z. L. Rotary Triboelectric Nanogenerator Based on a Hybridized Mechanism for Harvesting Wind Energy. *ACS Nano* **2013**, *7*, 7119–7125.
- (10) Liu, J.; Cui, N.; Gu, L.; Chen, X.; Bai, S.; Zheng, Y.; Hu, C.; Qin, Y. A Three-dimensional Integrated Nanogenerator for Effectively Harvesting Sound Energy from the Environment. *Nanoscale* **2016**, *8*, 4938–4944.
- (11) Cui, N.; Gu, L.; Liu, J.; Bai, S.; Qiu, J.; Fu, J.; Kou, X.; Liu, H.; Qin, Y.; Wang, Z. L. High Performance Sound Driven Triboelectric Nanogenerator for Harvesting Noise Energy. *Nano Energy* **2015**, *15*, 321–328.
- (12) Chen, J.; Zhu, G.; Yang, W.; Jing, Q.; Bai, P.; Yang, Y.; Hou, T.-C.; Wang, Z. L. Harmonic-Resonator-Based Triboelectric Nanogenerator as a Sustainable Power Source and a Self-Powered Active Vibration Sensor. *Adv. Mater.* **2013**, *25*, 6094–6099.
- (13) Gu, D.; Li, X.; Wang, H.; Li, M.; Xi, Y.; Chen, Y.; Wang, J.; Rumyantseva, M. N.; Gaskov, A. M. Light Enhanced VOCs Sensing of WS_2 Microflakes Based Chemiresistive Sensors Powered by Triboelectric Nanogenerators. *Sens. Actuators, B* **2018**, *256*, 992–1000.
- (14) Liu, G.; Nie, J.; Han, C.; Jiang, T.; Yang, Z.; Pang, Y.; Xu, L.; Guo, T.; Bu, T.; Zhang, C.; Wang, Z. L. Self-Powered Electrostatic Adsorption Face Mask Based on a Triboelectric Nanogenerator. *ACS Appl. Mater. Interfaces* **2018**, *10*, 7126–7133.
- (15) Starner, T. Human-Powered Wearable Computing. *IBM Syst. J.* **1996**, *35*, 618–629.
- (16) Qi, Y.; McAlpine, M. C. Nanotechnology-Enabled Flexible and Biocompatible Energy Harvesting. *Energy Environ. Sci.* **2010**, *3*, 1275–1285.
- (17) Adame, T.; Bel, A.; Bellalta, B.; Barcelo, J.; Oliver, M. IEEE 802.11ah: The Wi-Fi Approach for M2M Communications. *IEEE Wireless Commun.* **2014**, *21*, 144–152.
- (18) Somavat, P.; Jadhav, S.; Namboodiri, V. Accounting for the Energy Consumption of Personal Computing Including Portable Devices. Proceedings of the 1st International Conference on Energy-Efficient Computing and Networking, ACM, 2010; 141–149.
- (19) Wu, C.; Wang, A. C.; Ding, W.; Guo, H.; Wang, Z. L. Triboelectric Nanogenerator: A Foundation of the Energy for the New Era. *Adv. Funct. Mater.* **2019**, *9*, No. 1802906.

- (20) Wang, A. C.; Wu, C.; Pisignano, D.; Wang, Z. L.; Persano, L. Polymer Nanogenerators: Opportunities and Challenges for Large-Scale Applications. *J. Appl. Polym. Sci.* **2018**, *135*, 45674.
- (21) Zhu, G.; Pan, C.; Guo, W.; Chen, C.-Y.; Zhou, Y.; Yu, R.; Wang, Z. L. Triboelectric-Generator-Driven Pulse Electrodeposition for Micropatterning. *Nano Lett.* **2012**, *12*, 4960–4965.
- (22) Cui, N.; Liu, J.; Gu, L.; Bai, S.; Chen, X.; Qin, Y. Wearable Triboelectric Generator for Powering the Portable Electronic Devices. *ACS Appl. Mater. Interfaces* **2015**, *7*, 18225–18230.
- (23) Chen, J.; Guo, H.; Pu, X.; Wang, X.; Xi, Y.; Hu, C. Traditional Weaving Craft for One-Piece Self-Charging Power Textile for Wearable Electronics. *Nano Energy* **2018**, *50*, 536–543.
- (24) Pu, X.; Guo, H.; Chen, J.; Wang, X.; Xi, Y.; Hu, C.; Wang, Z. L. Eye Motion Triggered Self-Powered Mechnosensational Communication System Using Triboelectric Nanogenerator. *Sci. Adv.* **2017**, *3*, No. e1700694.
- (25) Guo, H.; Pu, X.; Chen, J.; Meng, Y.; Yeh, M.-H.; Liu, G.; Tang, Q.; Chen, B.; Liu, D.; Qi, S.; Wu, C.; Hu, C.; Wang, J.; Wang, Z. L. A Highly Sensitive, Self-Powered Triboelectric Auditory Sensor for Social Robotics and Hearing Aids. *Sci. Robot.* **2018**, *3*, No. eaat2516.
- (26) Liu, W.; Wang, Z.; Wang, G.; Liu, G.; Chen, J.; Pu, X.; Xi, Y.; Wang, X.; Guo, H.; Hu, C.; Wang, Z. L. Integrated Charge Excitation Triboelectric Nanogenerator. *Nat. Commun.* **2019**, *10*, No. 1426.
- (27) Lee, S.; Ko, W.; Oh, Y.; Lee, J.; Baek, G.; Lee, Y.; Sohn, J.; Cha, S.; Kim, J.; Park, J.; Hong, J. Triboelectric Energy Harvester Based on Wearable Textile Platforms Employing Various Surface Morphologies. *Nano Energy* **2015**, *12*, 410–418.
- (28) Wang, X.; Wen, Z.; Guo, H.; Wu, C.; He, X.; Lin, L.; Cao, X.; Wang, Z. L. Fully Packaged Blue Energy Harvester by Hybridizing a Rolling Triboelectric Nanogenerator and an Electromagnetic Generator. *ACS Nano* **2016**, *10*, 11369–11376.
- (29) Chun, J.; Ye, B. U.; Lee, J. W.; Choi, D.; Kang, C.-Y.; Kim, S.-W.; Wang, Z. L.; Baik, J. M. Boosted Output Performance of Triboelectric Nanogenerator via Electric Double Layer Effect. *Nat. Commun.* **2016**, *7*, No. 12985.
- (30) Zhang, L.; Cheng, L.; Bai, S.; Su, C.; Chen, X.; Qin, Y. Controllable Fabrication of Ultrafine Oblique Organic Nanowire Arrays and Their Application in Energy Harvesting. *Nanoscale* **2015**, *7*, 1285–1289.
- (31) Fan, F.-R.; Lin, L.; Zhu, G.; Wu, W.; Zhang, R.; Wang, Z. L. Transparent Triboelectric Nanogenerators and Self-Powered Pressure Sensors Based on Micropatterned Plastic Films. *Nano Lett.* **2012**, *12*, 3109–3114.
- (32) Zhu, G.; Lin, Z.-H.; Jing, Q.; Bai, P.; Pan, C.; Yang, Y.; Zhou, Y.; Wang, Z. L. Toward Large-Scale Energy Harvesting by a Nanoparticle-Enhanced Triboelectric Nanogenerator. *Nano Lett.* **2013**, *13*, 847–53.